Supporting Information

Highly Coordinative Molecular Cobalt-Phthalocyanine Electrocatalyst on Oxidized Single-Walled Carbon Nnotubes for Efficient Hydrogen Peroxide Production

Yaoxin Li, [ab] Haoying Cheng, [bc] Meilin Wang, [bc] Jiaoxing Xu [ab*] Lunhui Guan [ab*]

a. College of Chemistry, Fuzhou University, Fuzhou, Fujian 350007, China.

b. CAS Key Laboratory of Design and Assembly of Functional Nanostructures, Fujian Provincial Key Laboratory of Nanomaterials, Fujian Institute of Research on the Structure of Matter, Chinese Academy of Sciences, Fuzhou, Fujian 350108, China.

c. College of Chemistry and Materials Science, Fujian Normal University, Fuzhou, Fujian 350007, China.

Correspondence should be addressed to: Jiaoxing Xu and Lunhui Guan, Fujian Institute of Research on the Structure of Matter, Chinese Academy of Sciences, YangQiao Road West 155, Fuzhou, Fujian 350002, P.R. China. Email: xujx_1220@fjirsm.ac.cn, guanlh@fjirsm.ac.cn.

Supplemental Experimental Procedures

Chemicals

The precursors of Single-walled carbon nanotubes (SWCNTs) and Cobalt phthalocyanine (CoPc) were purchased from Ocsial and Adamas-beta respectively. Concentrated H_2SO_4 (98.4%), HCl (37%), H_2O_2 (30%), N, N-dimethylformamide (DMF) and $KMnO_4$ powder were purchased from Sinopharm Chemical Reagent Co., Ltd. (Shanghai, China) and used without further purification.

Material synthesis

Synthesis of *o*-SWCNT-2. The synthesis of *o*-SWCNT-2 was conducted following the traditional Hummers' method[1]. Briefly, 200 mg of single-walled carbon nanotubes (SWCNTs) and 400 mg of $KMnO_4$ powder were dispersed into 30 mL H_2SO_4 (98.4%), the mixture was transferred into an oil bath set at 50 °C and stirred for 3 hours. After an ice bath, the product was diluted to 150 ml using deionized water and 10 mL of H_2O_2 (30%) solution was added to the mixture and reacted for 15 minutes. Then, the precipitate was collected by filtration and washed with 150 ml of HCl solution (the volume ratio of HCl to H_2O was 1:9) to completely eliminate metal clusters. After filtering, the final solid sample was homogeneously dispersed in 200 mL of deionized water. Then, the homogeneous dispensation was centrifugated at 13,500 rpm for 30 minutes, leading to solid-liquid separation. The upper liquid was carefully removed and the centrifugation process was repeated until a neutral pH was reached in upper liquid. The precipitate obtained by centrifugation was dispersed in 200 ml of deionized water and sonicated for 15 minutes. Subsequently, the slurry was centrifuged again at 13500 rpm for 30 minutes and the upper brown solution was collected as *o*-SWCNT-2.

Synthesis of CoPc-Xwt%/*o*-SWCNT-2. 30 mg of *o*-SWCNT-2 and a calculated amount of CoPc (0, 1, 3, 6, 9 wt%) were dispersed in 30 ml of DMF solution with sonication for 30 minutes respectively. Subsequently, both of them were mixed with sonication for another 30 minutes to obtain a well-mixed dispersion. The CoPc-Xwt%/*o*-SWCNT-2 electrocatalysts were obtained by stirred the mixing

dispersion for 24 h and followed by a freeze-drying process.

Synthesis of CoPc-6wt%/*o*-SWCNT-Y. The feeding ratio of $KMnO_4$ and SWCNT powder was adjusted from 1 to 3 to obtain *o*-SWCNT-Y (Y indicates $KMnO_4$/SWCNT, Y=1, 2 and 3) with different oxidative degree. The as-prepared *o*-SWCNT-Y support were used to fabricate CoPc-6wt%/*o*-SWCNT-Y in same process.

Characterization

Field emission scanning electron microscopy (FE-SEM, SU8010), transmission electron microscopy (TEM), high-resolution TEM (HR-TEM) and high-angle annular dark-field scanning TEM (HAADF-STEM) were performed to analyze the morphology and microstructure of catalysts. Aberration-corrected high-angle annular dark-field scanning transmission electron microscopy (HAADF-STEM, JEM-ARM300F) was used to analyze the single atom structure of catalysts. Co *K*-edge X-ray absorption near-edge structure (XANES) and extended X-ray absorption fine structure (EXAFS) analyses were used to determine the electronic structure and local coordination of Co in the catalysts. X-ray diffraction (XRD) characterization was performed on a Miniflex 600 diffractometer with Cu Kα X-rays (1.5406 Å). The surface chemical states of the samples were investigated through X-ray photoelectron spectroscopy (XPS, ESCALAB 250 Xi). The Co concentration on catalysts was evaluated on the Inductively coupled plasma optical emission spectroscopy [ICP-OES, NexION 2000-(A-10)].

Electrochemical measurements

The electrochemical performance for $2e^-$ ORR of various catalysts was investigated using the CHI760E electrochemical workstation (Shanghai CH Instruments, Inc., China) with a three-electrode configuration system at room temperature. A high-purity graphite rod and Ag/AgCl electrode with saturated KCl salt bridge were used as the counter electrode and reference electrode respectively. The

Rotating Ring Disk Electrode (RRDE) is composed of glassy carbon disk electrode (0.2475 cm^2) and Pt ring electrode (0.1866 cm^2). The homogeneous catalyst ink was prepared by dispersing 3 mg of as-prepared catalyst powder in a solution containing 60 μL of Nafion (5 wt%) and 540 μL of isopropanol with sonication at least 30 minutes. The well-dispersed ink was then dropped on glassy carbon disk electrode with a loading of 0.1 mg cm^{-2}. Before the electrochemical measurement, the pre-activation was conducted by scanning cycle voltammetry (CV) curves (60 cycles, scan rate: 10 mV/s) in O_2-saturated 0.1 M K_2SO_4 electrolyte until stable CV curves were obtained. The linear sweep voltammetry (LSV) curves of the catalysts were measured with various rotation rate of 500, 900, 1200, 1600, 2000 and 2500 rpm (scan rate: 10 mV/s) and electrode potentials were converted to the reversible hydrogen electrode (RHE) using the equation *S1*. The H_2O_2 selectivity and electro transfer number (n) were calculated by the following equation *S2* and *S3*. Moreover, the n of CoPc-6wt%/o-SWCNT-2 was calculated by the Koutecky-Levich (K-L) equation *S4* and *S5*.

$$E(RHE) = E(Ag/AgCl) + 0.059 \times pH + 0.197 \quad (S1)$$

$$n = 4 \times I_D / (I_D \times N + I_R) \quad (S2)$$

$$Selectivity\,(H_2O_2)\,\% = 200 \times I_R / (I_D \times N + I_R) \quad (S3)$$

$$\frac{1}{j} = \frac{1}{j_k} + \frac{1}{j_d} = \frac{1}{j_k} + \frac{1}{B\omega^{1/2}} \quad (S4)$$

$$K = 0.62nFC_0D_{O_2}v^{-1/6} \quad (S5)$$

Where, the I_D is the disk current, and the I_R is the ring current; j indicates the measured current density, j_d is the kinetic current density; j_K is the diffusion-limiting current density; ω is the angular velocity of the disk (rpm min^{-1}); n is the number of electrons transferred in the ORR; F is the for Faraday constant (96485 C mol^{-1}). C_0 and D_{O2} is the bulk concentration of O_2 (1.2×10^{-6} mol cm^{-3}) and diffusion coefficient of O_2 (1.9×10^{-5} cm^2 s^{-1}), respectively; v is the kinematic viscosity of the electrolyte (0.01 cm^2 s^{-1}); the above parameters are determined under the standard atmospheric pressure of 25 ℃.

The EIS was evaluated in O_2-saturated 0.1 M K_2SO_4 electrolyte using the Zahner electrochemical workstation. The test voltage and disturbance voltage were set at 0.1 V vs. RHE and 5 mV in a frequency range from 100 kHz to 10 mHz.

Bulk electrosynthesis and electro-Fenton degradation of a model organic pollutant on CoPc-6wt%/*o*-SWCNT-2 catalyst

The H_2O_2 yield was measured in O_2-saturated 0.1 M K_2SO_4 electrolyte in H-cell device where cathode and anode chamber were separated by the nafion-212 membrane. Pt wire and Ag/AgCl electrode were used as the counter and reference electrode, respectively. The gas diffusion electrode (GDE) was made by coating 0.1 mg cm^{-2} catalyst on 1 cm^2 carbon paper. The chronoamperometry (i-t) curves for 0.5 h at various potentials (0.1, 0.2 and 0.3 V vs. RHE) were captured and the cathode potential was maintained at 0.1 V vs. RHE to test the stability of catalyst.

The H_2O_2 production rate was further measured in Flow-cell device in O_2-saturated 1 M Na_2SO_4. The ink of catalyst was dropped on 2 cm^2 carbon paper with a loading of 0.1 mg cm^{-2}. During the test, the recycled rate of electrolyte and O_2 supply rate were maintained at 5 ml min^{-1} and 25 ml min^{-1}, respectively. The H_2O_2 concentration was measured by traditional $KMnO_4$ titration method according to Chinese national standard GB/T23499-2009[2]. The concentration of H_2O_2 production and faradaic efficiency (FE) were calculated by the following equation *S6* and *S7*.

$$C_{H_2O_2} = 5 \times C_{KMnO_4} \times V_{KMnO_4} \div 2V_{H_2O_2} \qquad (S6)$$

$$FE\,(\%) = 2CVF / Q\,(\%) \qquad (S7)$$

Where C is the H_2O_2 concentration (mol L^{-1}), V represents the volume of electrolyte (L), F indicates the faraday constant (96485 C mol^{-1}), Q is the consumed charge amount (C).

Turnover frequency (TOF) calculation for H_2O_2 electrosynthesis. TOF signifies the quantity of O_2 converted into the objective H_2O_2 by a single active site per time. The TOF equations were derived as

follows.

$$TOF\left(s^{-1}\right)=\frac{TON_{O_2}}{n}=\frac{j/2F}{n} \qquad (S8)$$

$$(\mathrm{TON_{O2}}) = \mathrm{j}\left[\frac{\mathrm{A}}{\mathrm{cm}^2}\right]\times \mathrm{FE}\times\frac{1[C/s]}{1[A]}\times\frac{1[mol\ e^-]}{96485[C]}\times\frac{1[mol\ O_2]}{2[mol\ e^-]}\times\left(6.02\times10^{23}\left[\frac{atom\ O_2}{mol\ O_2}\right]\right) \qquad (S9)$$

$$n = M\left[\frac{mg}{\mathrm{cm}^2}\right]\times R\ [\mathrm{wt\%}]\times\frac{1\left[mmol\right]}{W\left[mg\right]}\times\left(6.02\times10^{20}\left[\frac{atom\ O_2}{mol\ O_2}\right]\right) \qquad (S10)$$

Where, the j is cathode catalytic current density, F represents the faraday constant (96,485 C mol^{-1}), FE indicates the Faradaic efficiency of H_2O_2 production, n signifies the number of active sites. CoPc-6wt%/*o*-SWCNT-2 was taken as an example.

$$\text{- } (\mathrm{TON_{O2}}) = 0.04\left[\frac{\mathrm{A}}{\mathrm{cm}^2}\right]\times 0.73\times\frac{1[C/s]}{1[A]}\times\frac{1[mol\ e^-]}{96485[C]}\times\frac{1[mol\ O_2]}{2[mol\ e^-]}\times\left(6.02\times10^{23}\left[\frac{atom\ O_2}{mol\ O_2}\right]\right)=9.1\times10^{16}\left[\frac{atom\ O_2}{mol\ O_2}\right]$$

$$\text{- (number of CoPc site)} = 0.1\left[\frac{mg}{\mathrm{cm}^2}\right]\times 0.0036\times\frac{1\left[mmol\right]}{58.933\left[mg\right]}\times\left(6.02\times10^{20}\left[\frac{atom\ O_2}{mol\ O_2}\right]\right)=3.6\times10^{15}\left[\frac{atom\ O_2}{mol\ O_2}\right]$$

Electron-Fenton degradation test was performed in O_2-saturated 0.1 M acidified K_2SO_4 solution (pH 2~3) in H-cell device at 0.1 V vs. RHE. To prepared working electrode, 0.1 mg CoPc-6wt%/*o*-SWCNT-2 catalyst ink was deposited on 1 cm^2 carbon paper. MB (50 mg/L) and Fe^{2+} (0.5 mM) were added to the electrolyte on the working electrode side. A portion of electrolyte was taken from cathode chamber every 5 minutes and the MB concentration of electrolyte was determined by UV-vis spectrophotometry.

DFT Calculation methods and details.

We performed the density functional theory (DFT) based calculations[3] by using the Vienna Ab initio Simulation Package (VASP),[4, 5] which enabled us to achieve the relaxed geometries and total energies. We adopted the projector augmented wave (PAW)[6] method describe the nuclei-electron interactions. The Perdew-Burke-Ernzerhof (PBE) functional within the generalized gradient approximation (GGA)[7] was employed to calculate the exchange-correlation energy. the van der Waals (vdW) correction proposed by Grimme (DFT-D3) was employed due to its good description of long-range vdW interactions.[8] The vacuum space was set to larger than 15 Å in the z direction to avoid

interactions between periodic images. The kinetic cutoff energy was set to 500 eV. In addition, the plane wave basis expansion with force was set as 0.02 eV/Å on each atom for the convergence criterion of geometry relaxation. All the surface calculation was performed by the 3×3×1 Monkhorst-Pack grid k-points mesh.

Here, we used computational hydrogen electrode (CHE) model proposed by Nørskov et al. to calculate the free energy levels of all intermediates:[9]

$$\Delta G_{\text{ads}} = \Delta E_{\text{ads}} + \Delta ZPE - T\Delta S + eU \qquad (S11)$$

where ΔE_{ads} is the binding energy of adsorption species HOO∗. ΔZPE, ΔS, U and e are the ZPE changes, entropy changes, applied potential at the electrode, and charge transferred. The contributions of each component for ΔGads were obtained from previous literature.[10]

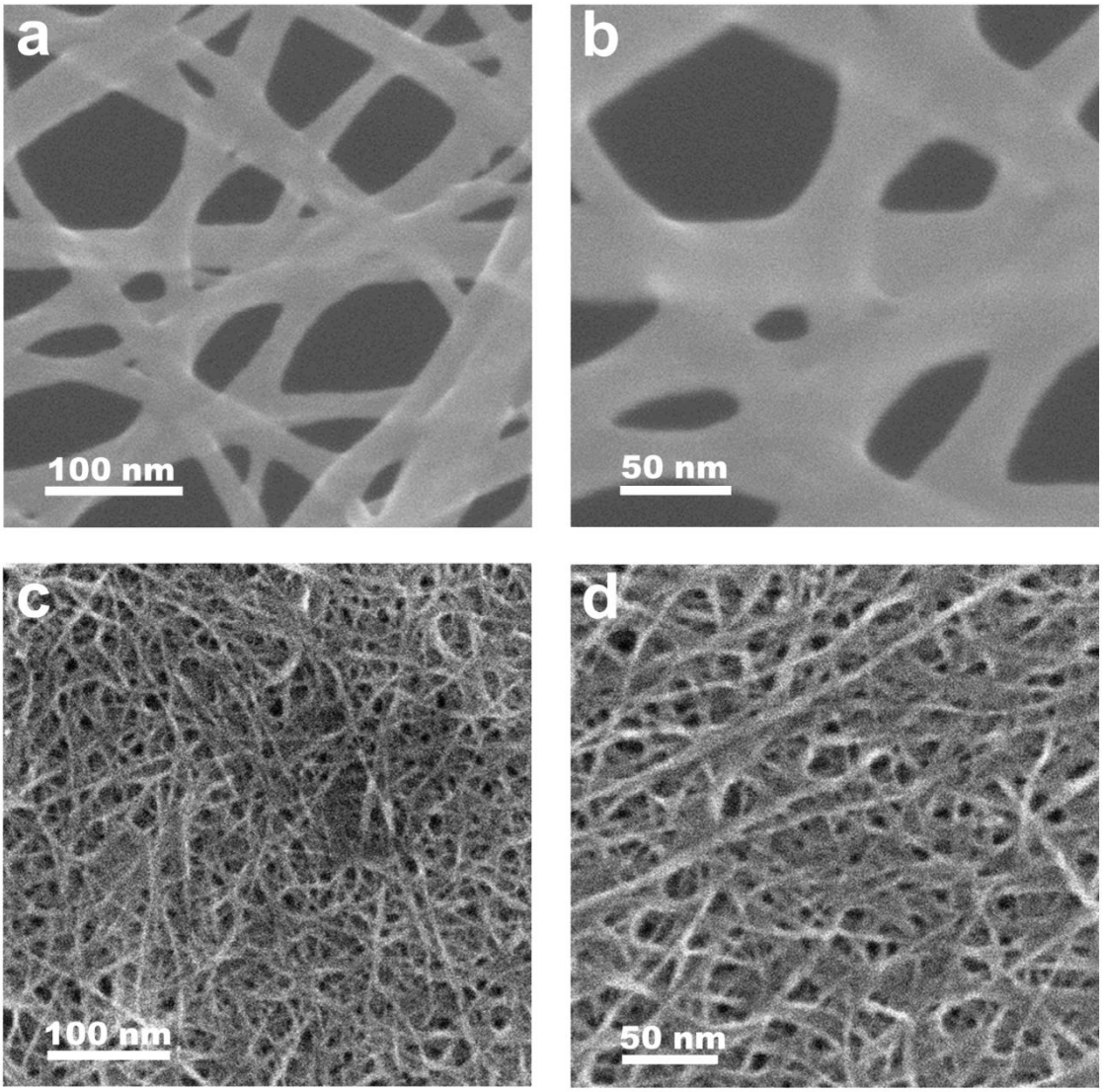

Fig. S1. The SEM images of original (a-b) SWCNT and (c-d) *o*-SWCNT-2.

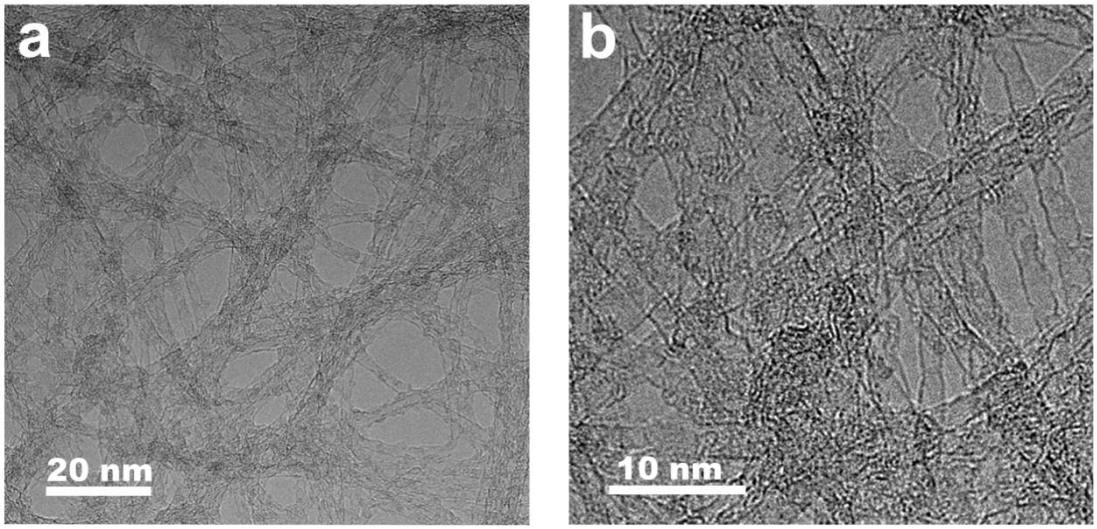

Fig. S2. (a-d) The HR-TEM images of *o*-SWCNT-2.

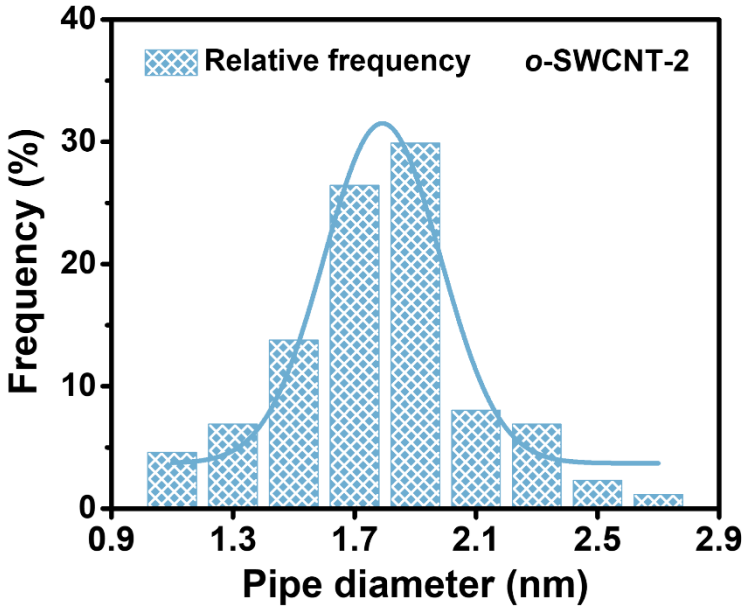

Fig. S3. The pipe-diameter distribution of *o*-SWCNT-2.

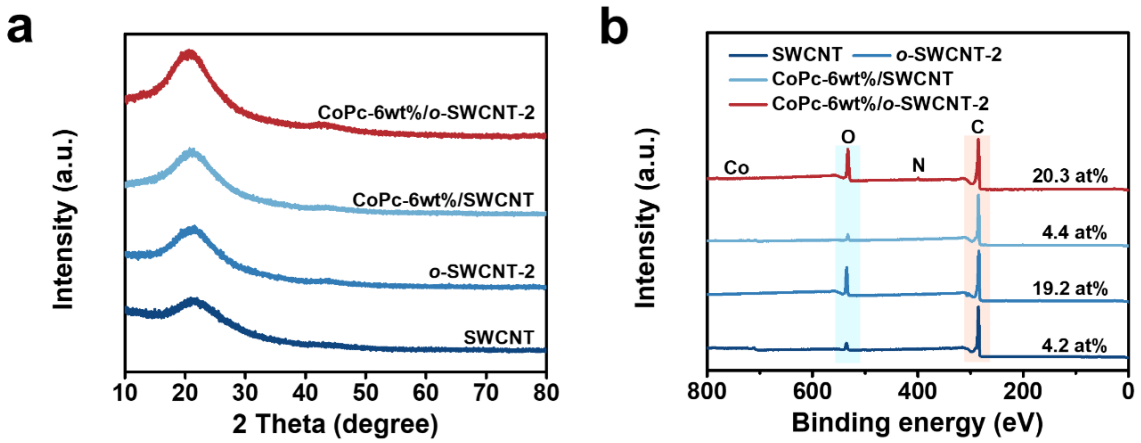

Fig. S4. (a-b) XRD patterns and XPS survey spectra of SWCNT, *o*-SWCNT-2, CoPc-6wt%/SWCNT and CoPc-6wt%/ *o*-SWCNT-2.

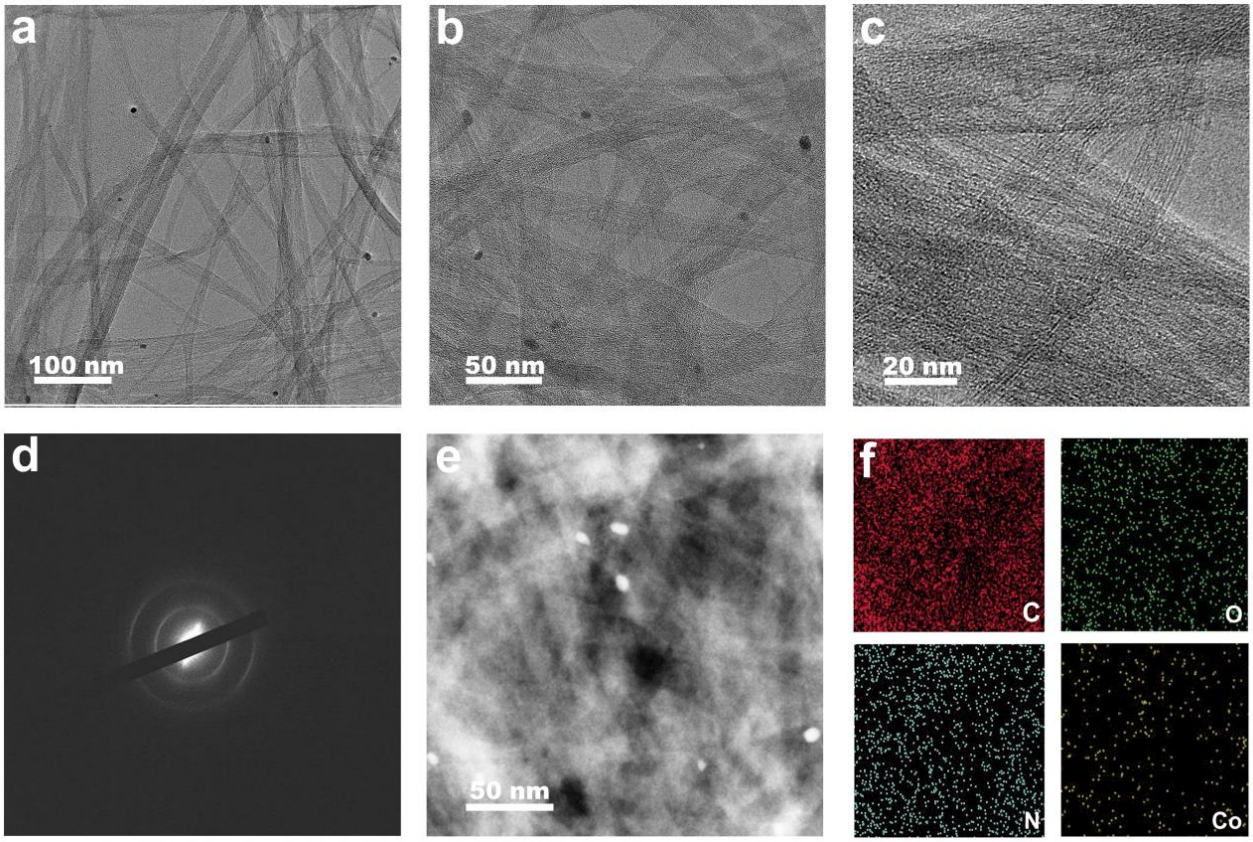

Fig. S5. (a-d) TEM, HR-TEM and EDX images of the CoPc-6wt%/*o*-SWCNT-1 catalyst; (e) The TEM-HAADF image and (f) Elemental mappings of C, O, N and Co.

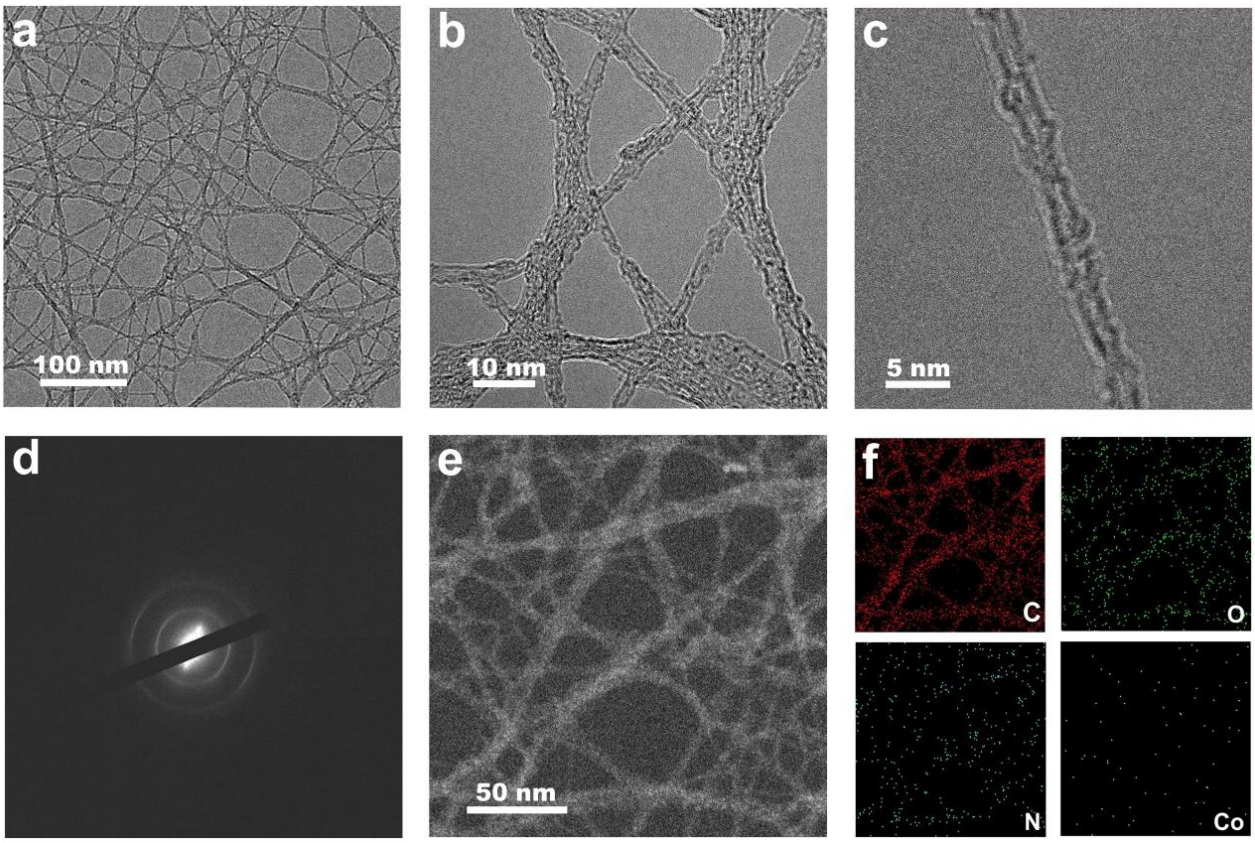

Fig. S6. (a-d) TEM, HR-TEM and EDX images of the CoPc-6wt%/*o*-SWCNT-3 catalyst; (e) The TEM-HAADF image and (f) Elemental mappings of C, O, N and Co.

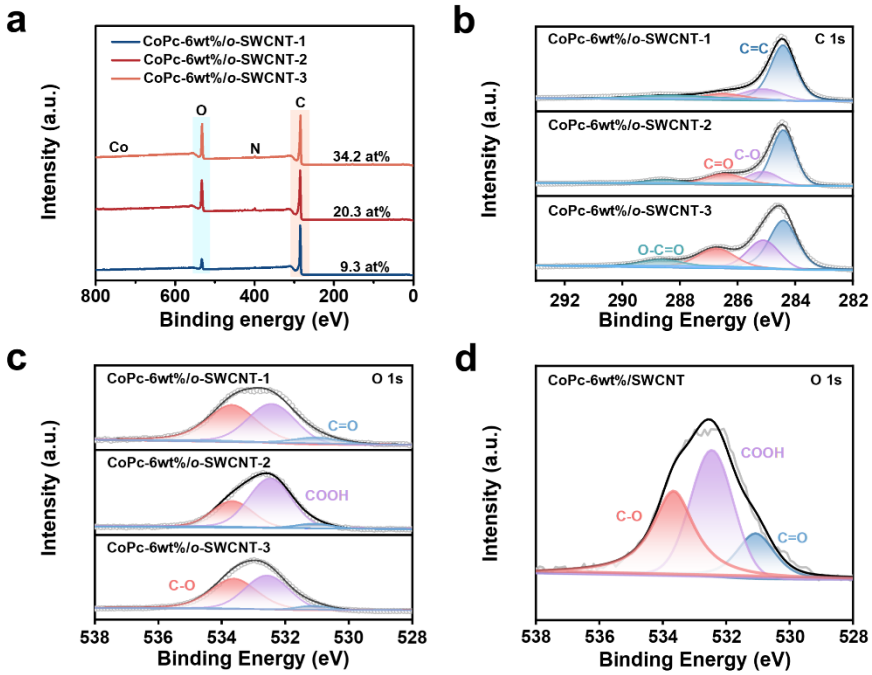

Fig. S7. (a) XPS survey spectra, (b) C *1s* high-resolution spectra and (c) O *1s* high-resolution spectra of CoPc-6wt%/*o*-SWCNT-1, CoPc-6wt%/*o*-SWCNT-2 and CoPc-6wt%/*o*-SWCNT-3. (d) O *1s* high-resolution spectra of CoPc-6wt%/SWCNT.

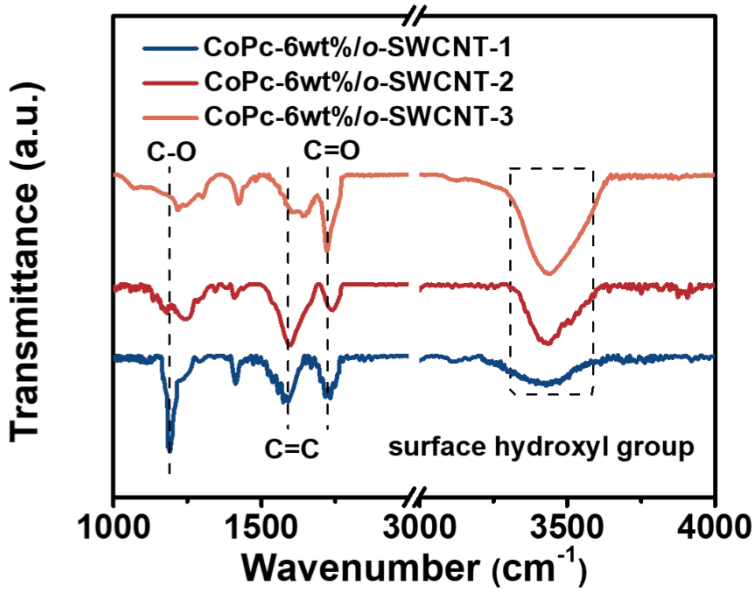

Fig. S8. (a) FT-IR spectrum of CoPc-6wt%/*o*-SWCNT-1, CoPc-6wt%/*o*-SWCNT-2 and CoPc-6wt%/*o*-SWCNT-3.

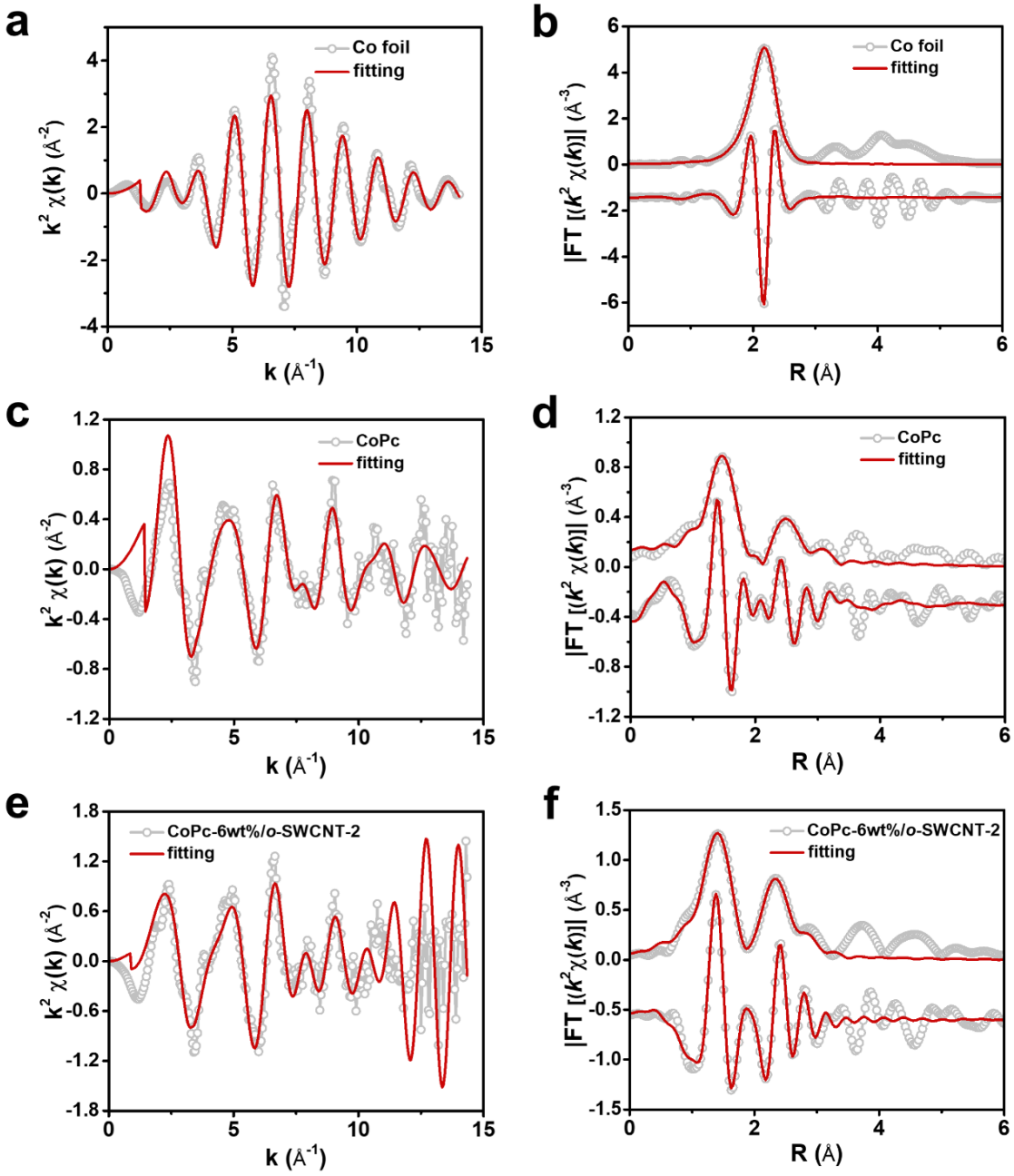

Fig. S9. (a-b) EXAFS analysis of Co foil at *K* space and *R* space, respectively. (c-d) EXAFS analysis of CoPc at *K* space and *R* space, respectively. (e-f) EXAFS analysis of CoPc-6wt%/*o*-SWCNT-2 at *K* space and *R* space, respectively.

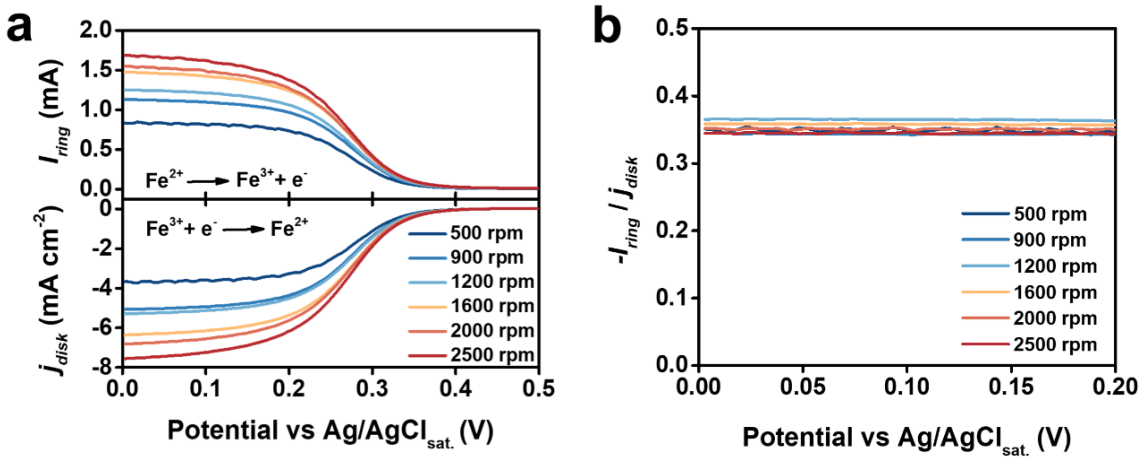

Fig. S10. Calibration of the collection efficiency of the RRDE by the redox of potassium ferricyanide.

Note: The collection efficiency (N) of the rotating ring-disk electrode (RRDE) was evaluated in 10 mM [$K_3Fe(CN)_6$] and 1 M KCl electrolyte with Pt plate as the counter electrode and Ag/AgCl electrode**.** To facilitate the reduction of Fe^{3+} to Fe^{2+}, the potential of the disk electrode was scanned in the range of 0.5 V to 0 V vs. Ag/AgCl. Conversely, the potential of the Pt ring was maintained at 0.5 V vs. Ag/AgCl to oxidize Fe^{2+} to Fe^{3+}. The collection efficiency (N) was calculated CE = - I_{Ring}/I_{Disk}, where I_{Ring} and I_{Disk} represent the current on Pt ring electrode and glassy carbon disk respectively.

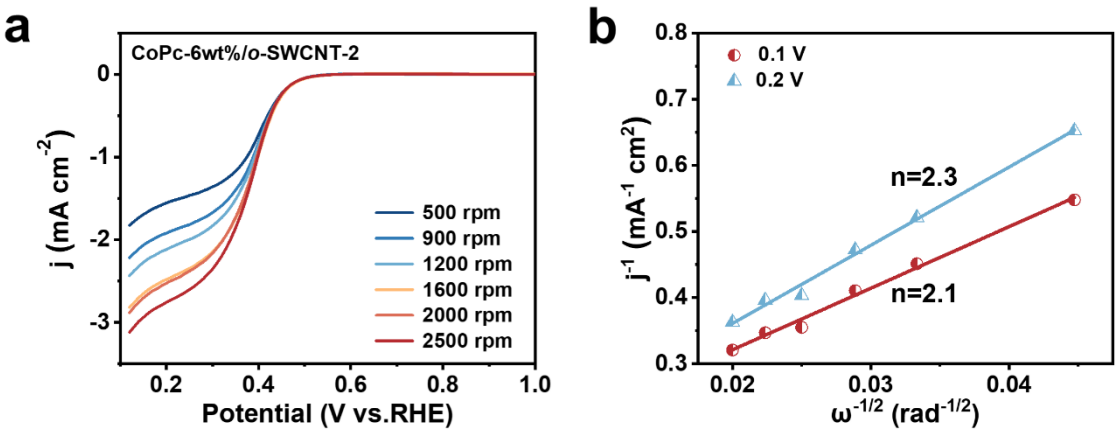

Fig. S11. (a) Lsv curves toward 2e$^-$ ORR of CoPc-6wt%/*o*-SWCNT-2 at various rotation speeds. (b) The calculated electron transfer number (*n*) at different potentials according to the Koutecky-Levich diffusion equation.

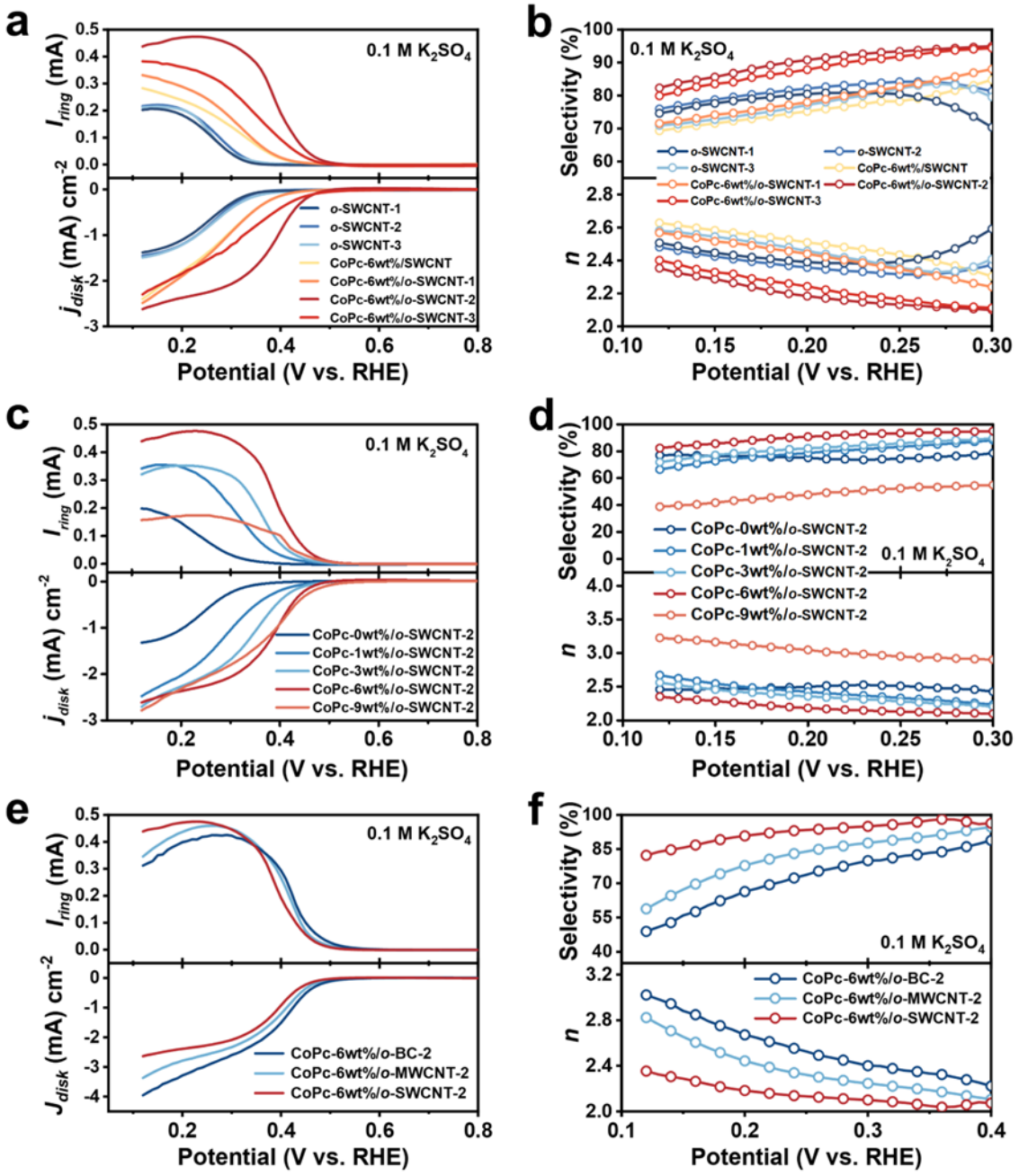

Fig. S12. (a) LSV curvers of *o*-SWCNT-1, *o*-SWCNT-2, *o*-SWCNT-3, CoPc-6wt%/SWCNT, CoPc-6wt%/*o*-SWCNT-1, CoPc-6wt%/*o*-SWCNT-2 and CoPc-6wt%/*o*-SWCNT-3 in O_2-saturated 0.1 M K_2SO_4 solution at 1600 rpm. (b) the corresponding H_2O_2 selectivity and electron transfer number (*n*). (c) LSV curvers of CoPc-0wt%/*o*-SWCNT-2, CoPc-1wt%/*o*-SWCNT-2, CoPc-3wt%/*o*-SWCNT-2, CoPc-6wt%/*o*-SWCNT-2 and CoPc-9wt%/*o*-SWCNT-2 in O_2-saturated 0.1 M K_2SO_4 solution at 1600 rpm. (d) the corresponding H_2O_2 selectivity and electron transfer number (*n*). (e) LSV curvers of CoPc-6wt%/*o*-SWCNT-2, CoPc-6wt%/*o*-MWCNT-2 and CoPc-6wt%/*o*-BC-2 in O_2-saturated 0.1 M K_2SO_4 solution at 1600 rpm. (f) the corresponding H_2O_2 selectivity and electron transfer number (*n*).

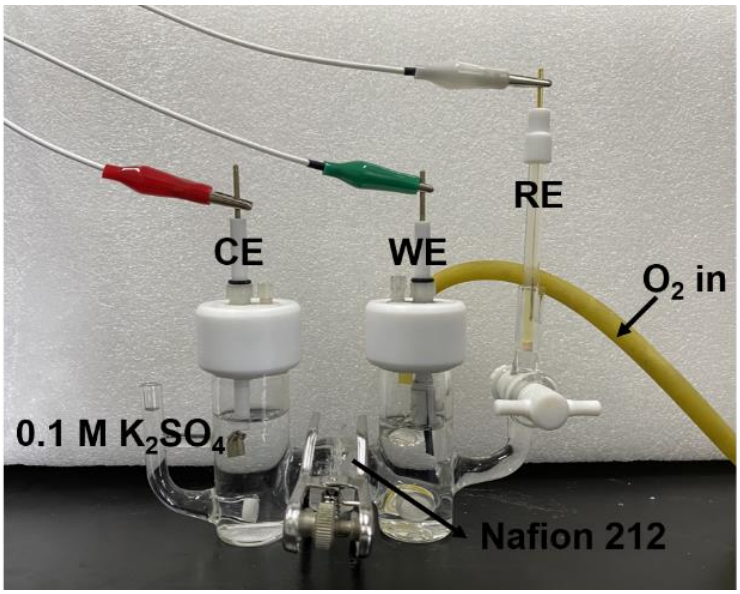

Fig. S13. The photograph of the H-cell device used in this study.

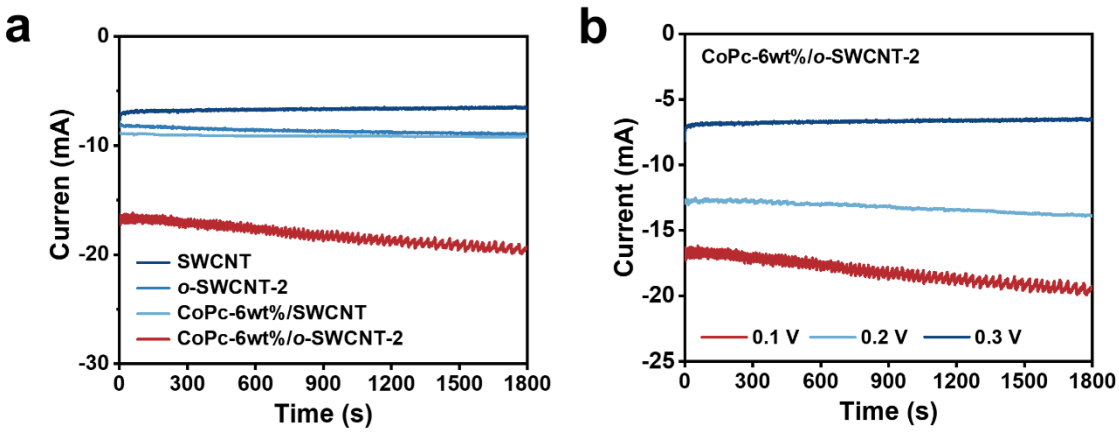

Fig. S14. (a) The chronoamperometry curves of SWCNT(O), *o*-SWCNT-2, CoPc-6wt%/SWCNT and CoPc-6wt%/*o*-SWCNT-2 in O_2-saturated 0.1 M K_2SO_4 electrolyte at 0.1 V for 1800s. (b) The chronoamperomety curves of CoPc-6wt%/*o*-SWCNT-2 in O_2-saturated 0.1 M K_2SO_4 electrolyte at different potentials (0.1, 0.2 and 0.3 V) for 1800s.

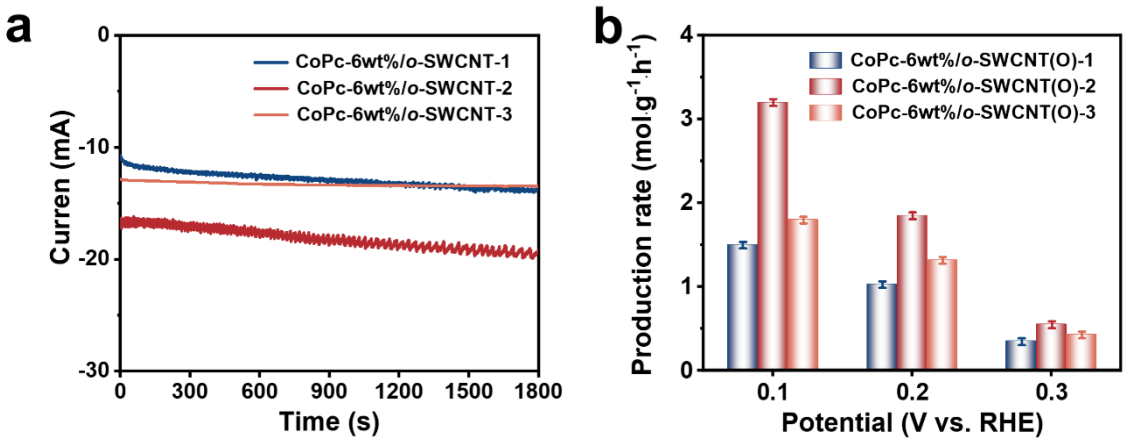

Fig. S15. (a) The chronoamperometry curves of CoPc-6wt%/*o*-SWCNT-1, CoPc-6wt%/*o*-SWCNT-2 and CoPc-6wt%/*o*-SWCNT-3 in O_2-saturated 0.1 M K_2SO_4 electrolyte at 0.1 V for 1800s. (b) The corresponding H_2O_2 production rate and Faradaic efficiency of three catalysts.

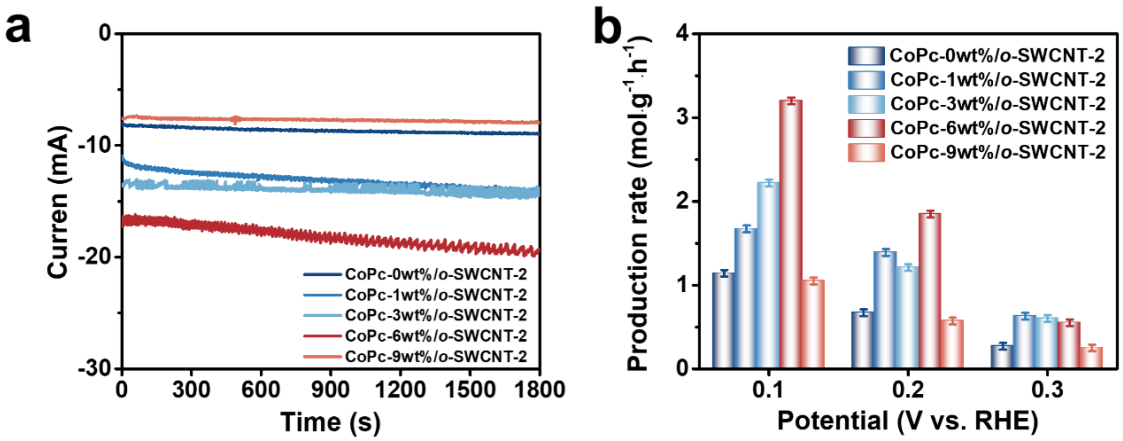

Fig. S16. (a) The chronoamperometry curves of CoPc-0wt%/*o*-SWCNT-2, CoPc-1wt%/*o*-SWCNT-2, CoPc-3wt%/*o*-SWCNT-2, CoPc-6wt%/*o*-SWCNT-2 and CoPc-9wt%/*o*-SWCNT-2 in O_2-saturated 0.1 M K_2SO_4 electrolyte at 0.1 V for 1800s. (b) The corresponding H_2O_2 production rate plots of five catalysts.

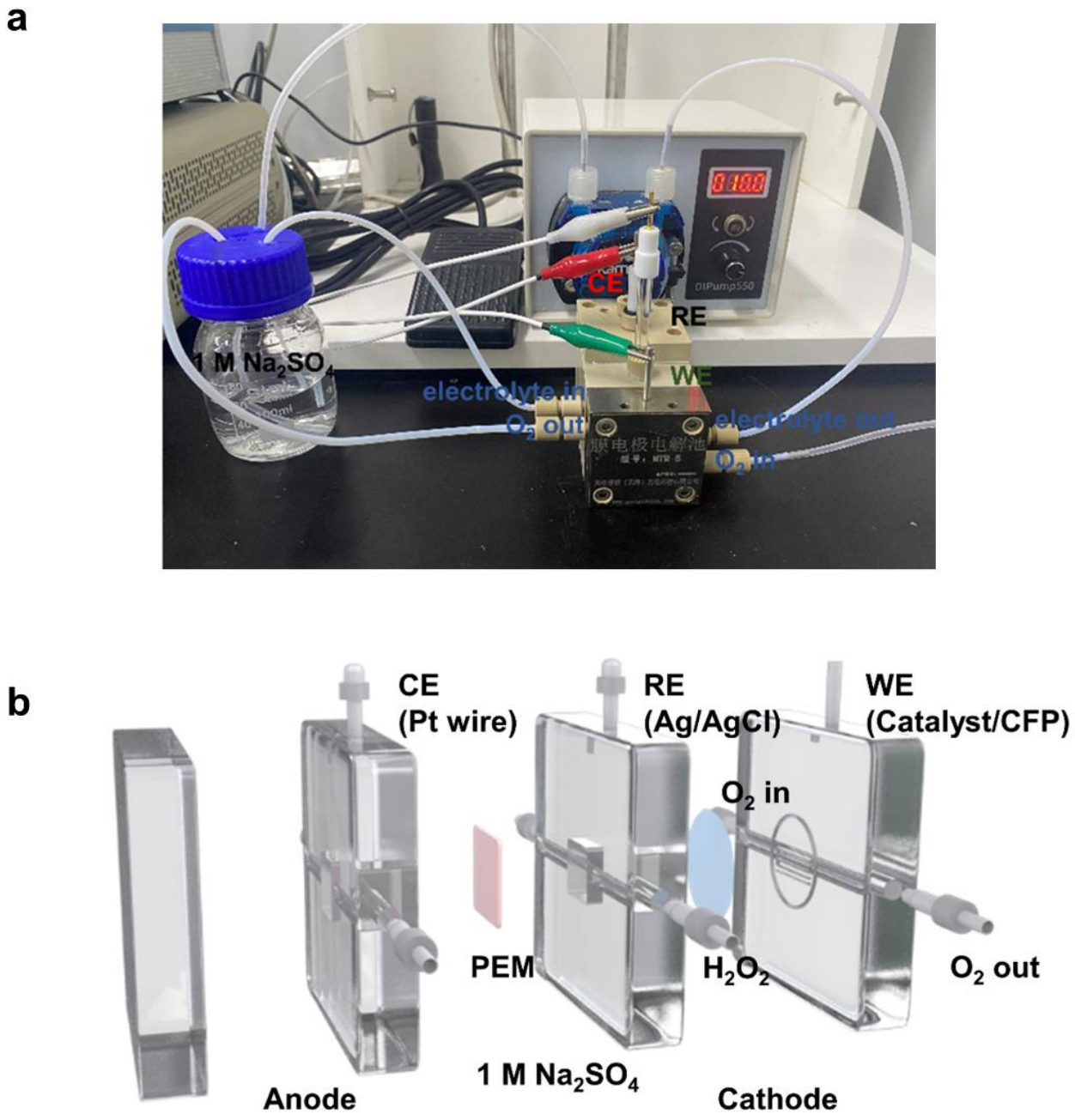

Fig. S17. The photograph and schematic diagram of the Flow-cell device used in this study.

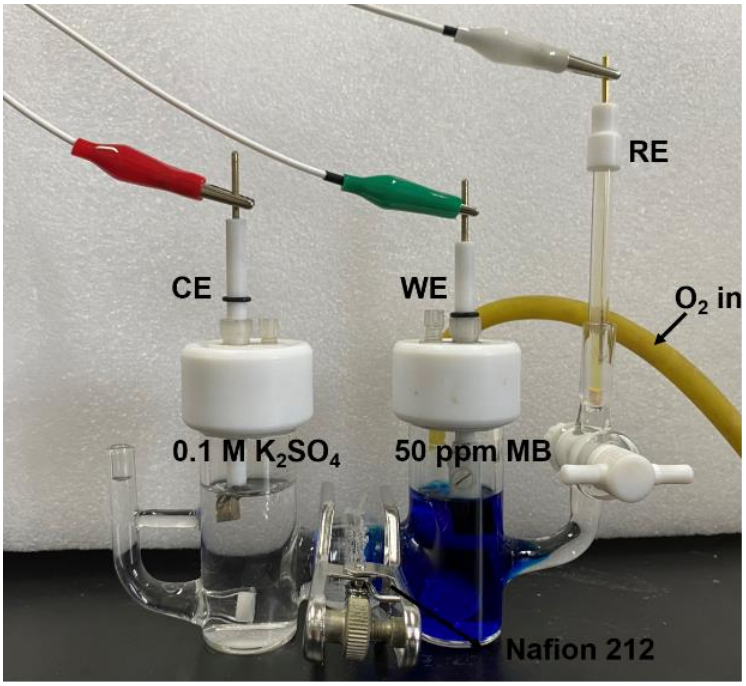

Fig. S18. The photograph of the Electro-Fenton device used in this study.

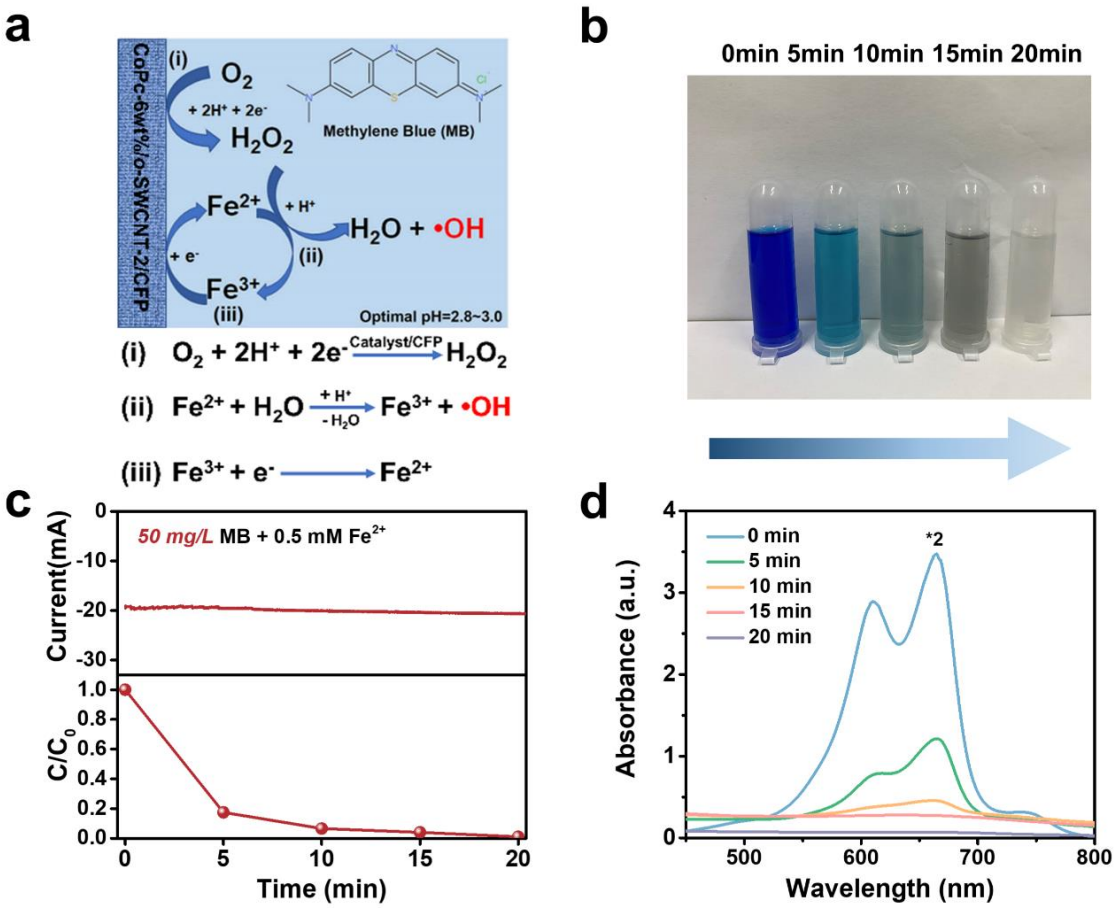

Fig. S19. (a) Schematic illustrations of the Electro-Fenton (EF) reaction process using CoPc-6wt%/*o*-SWCNT-2 as a cathodic catalyst. (b) The photograph of colour fade during the electro-Fenton mineralization. (c) The recorded chronoamperometry curve (Up) and the decay of the MB concentrations over time (Down). (d) The UV-vis absorption spectra of the MB solution.

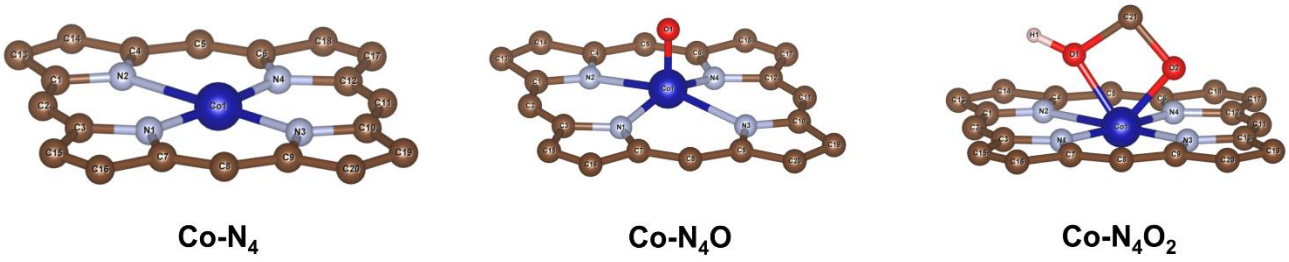

Fig. S20. Bader charge atom serial number of Co-N_4, Co-N_4O and Co-N_4O_2 models.

Table S1. EXAFS fitting parameters at the Co *K*-edge for the CoPc-6wt%/*o*-SWCNT-2, CoPc and Co foil samples.

Catalyst	Path	CN[a]	R (Å) [b]	σ² (Å⁻²) [c]	ΔE₀ (eV) [d]	R factor[e]
CoPc-6wt%/ *o*-SWCNT-2	Co-N_1	4.1±0.1	1.887±0.005	0.0018±0.0008	3.83±0.28	0.0065
	Co-O_1	1.9±0.1	2.429±0.014	0.0027±0.0024		
	Co-C_2	8.4±0.8	2.892±0.008	0.0016±0.0009		
	Co-N_2	4.5±1.0	3.288±0.018	0.0041±0.0026		
CoPc	Co-N_1	3.4±0.1	1.907±0.002	0.0013±0.0006	7.28±0.35	0.0040
	Co-C_2	8.3±0.3	2.943±0.003	0.0111±0.0082		
	Co-N_2	4.0±0.3	3.258±0.007	0.0020±0.0013		
Co foil	Co-Co	12[f]	2.486±0.003	0.0043±0.0002	5.52±0.12	0.0028

[a]*CN*: coordination numbers; [b]*R*: bond distance; [c]σ^2: Debye-Waller factors; [d]ΔE_0: the inner potential correction. [e]*R* factor: goodness of the fitting. The obtained XAFS data was processed in Athena (version 0.9.26) for background, pre-edge line and post-edge line calibrations. Then Fourier-transformed fitting was carried out in Artemis (version 0.9.26). S_0^2 was fixed as 0.5 for the fitting processes of CoPc-corresponding samples. The *k*-range of 2-10 $Å^{-1}$ and *R* range of 1-3 Å were used for the fitting of CoPc-corresponding samples. The *k*-range of 3 -12 $Å^{-1}$ and *R* range of 1-3 Å were used for the fitting of Co foil.

Table S2. The content of different elements for the six catalysts obtained from XPS measurements.

Sample	C (at%)	O (at%)	N (at%)	Co (at%)
SWCNT	94.59	4.22	1.14	0.05
o-SWCNT-2	70.39	19.22	1.37	0.02
CoPc-6wt%/SWCNT	93.86	4.44	1.55	0.15
CoPc-6wt%/*o*-SWCNT-1	89.02	9.29	1.57	0.12
CoPc-6wt%/*o*-SWCNT-2	77.29	20.29	2.20	0.22
CoPc-6wt%/*o*-SWCNT-3	63.58	34.26	2.79	0.39

Table S3. The proportion of different oxygen species of four catalysts obtained from XPS measurements.

Sample	C=O (%)	COOH (%)	C-O (%)
CoPc-6wt%/SWCNT	14.97	44.07	40.96
CoPc-6wt%/o-SWCNT-1	9.05	42.40	48.55
CoPc-6wt%/*o*-SWCNT-2	6.21	63.21	30.58
CoPc-6wt%/*o*-SWCNT-3	4.44	46.28	49.28

Table S4. The Co content of five catalysts obtained from ICP measurements.

Sample	Co content (wt%)	CoPc content (wt%)
CoPc-6wt%/SWCNT	0.28	2.71
CoPc-1wt%/*o*-SWCNT-2	0.07	0.67
CoPc-3wt%/*o*-SWCNT -2	0.11	1.07
CoPc-6wt%/*o*-SWCNT -2	0.36	3.59
CoPc-9wt%/*o*-SWCNT -2	0.41	3.97

Table S5. The EIS measurements of four catalysts.

Sample	$R_s(\Omega)$	$R_{ct}(\Omega)$	$R_w(\Omega)$
CoPc-6wt%/SWCNT	13	12.15	11.87
CoPc-6wt%/o-SWCNT-1	13.02	11.62	11.15
CoPc-6wt%/*o*-SWCNT -2	11.90	5.57	8.84
CoPc-6wt%/*o*-SWCNT -3	12.5	9.13	8.96

Table S6. Comparison of the $2e^-$ ORR H_2O_2 selectivity and with the recently reported transition-metallic SACs in neutral electrolyte.

Catalyst	Electrolyte	H_2O_2 selectivity (%)	Potential (V vs. RHE)	Ref.
CoPc-6wt%/*o*-SWCNT-2	**0.1M K_2SO_4**	**82 ~ 95**	**0.1 ~ 0.3**	**This work**
CoPc-CNT(O)	0.1M K_2SO_4	86 ~ 96	0.25 ~0.6	11
Co/NC	0.5 M NaCl	93.7	0.55	12
Fe-CNT	0.1 M PBS	80 ~ 97	0.1 ~ 0.5	13
O-C(Al)	0.1 M PBS	~ 90	0.1 ~ 0.45	14
$Cu_{0.1}$SA/CNNS	0.1 M PBS	90	0.3	15
$Ni_{0.1}$SA/CNNS	0.1 M PBS	98	0.3	
Cu/NCNSs	0.1 M PBS	~ 78	-0.1 ~ 0.4	16

Table S7. Comparison of the $2e^-$ ORR H_2O_2 yield rate and stability with the recently reported transition-metallic SACs in neutral electrolyte.

Catalyst	Electrolyte	Applied potential (V vs. RHE)	H_2O_2 yield rate ($mol \cdot g^{-1} \cdot h^{-1}$)	Stability (h)	Ref.
CoPc-6wt%/*o*-SWCNT-2	**1 M Na_2SO_4 (Flow cell)**	**0.1**	**5.85**	**20**	**This work**
	0.1 M K_2SO_4 (H-cell)	**0.1**	**3.12**	**75**	
CoPc-CNT(O)	1 M Na_2SO_4 (Flow cell)	3.1	26.1	100	11
Co/NC	0.5 M NaCl (Flow cell)	0.3	4.5	24	12
Fe-CNT	0.1 M PBS (H-cell)	0.36	0.65	6.5	13
O-C(Al)	0.5 M Na_2SO_4 (H-cell)	0.45	0.51	1	14
$Ni_{0.1}$SA/CNNS	0.1 M PBS (H-cell)	0.1	0.503	16	15
$Cu_{0.1}$SA/CNNS	0.1 M PBS (H-cell)	0.1	0.332	/	
Cu/NCNSs	0.1 M PBS (H-cell)	-0.2	0.204	30	16

Table S8. Summary of the TOF values of recently reported transition-metallic SACs for H_2O_2 electrosynthesis in neutral electrolyte.

Catalyst	Active sites	TOF (s^{-1})	Electrolyte	Ref.
CoPc-6wt%/*o*-SWCNT-2	**CoPc**	**25.2**	**1 M Na_2SO_4**	**This work**
CoPc-CNT(O)-1 wt%	CoPc	56	1 M Na_2SO_4	11
CoPc-CNT(O)-6 wt%	CoPc	18.5	1 M Na_2SO_4	
CoPc-CNT	CoPc	7	1 M Na_2SO_4	
O-Co-N_2C_2	Co	11.48	0.1 M PBS	17
Fe-CNT	Fe	1.96	0.1 M PBS	13
Co/NCNSs	Co	1.1	0.1 M PBS	16
Cu/NCNSs	Cu	1	0.1 M PBS	
COF-360-Co	TAPP-Co	0.95	0.1 M K_2SO_4	18

Table S9. Bader charge calculation results.

Serial number	Atoms	Charge variation of Co-N_4	Serial number	Atoms	Charge variation of Co-N_4O	Serial number	Atoms	Charge variation of Co-N_4O_2
1	N	0.97	1	N	0.95	1	N	0.91
2	N	1.09	2	N	1.05	2	N	1.04
3	N	1.02	3	N	1.05	3	N	0.96
4	N	0.99	4	N	0.95	4	N	0.84
5	C	-0.47	5	C	-0.42	5	C	-0.43
6	C	0.07	6	C	-0.10	6	C	0.04
7	C	-0.51	7	C	-0.35	7	C	-0.44
8	C	-0.49	8	C	-0.57	8	C	-0.49
9	C	0.00	9	C	0.02	9	C	0.06
10	C	-0.36	10	C	-0.38	10	C	-0.45
11	C	-0.36	11	C	-0.42	11	C	-0.35
12	C	0.05	12	C	0.05	12	C	0.01
13	C	-0.47	13	C	-0.51	13	C	-0.43
14	C	-0.38	14	C	-0.48	14	C	-0.37
15	C	0.21	15	C	0.11	15	C	-0.05
16	C	-0.61	16	C	-0.55	16	C	-0.41
17	C	-0.06	17	C	-0.10	17	C	-0.11
18	C	0.04	18	C	0.11	18	C	0.07
19	C	0.16	19	C	0.13	19	C	0.04
20	C	-0.03	20	C	0.04	20	C	0.14
21	C	0.11	21	C	0.22	21	C	0.13
22	C	0.05	22	C	-0.07	22	C	0.03
23	C	-0.10	23	C	0.08	23	C	-0.06
24	C	0.11	24	C	-0.06	24	C	0.02
25	Co	-1.03	25	Co	-1.26	25	C	-0.44
			26	O	0.50	26	Co	-1.31
						27	O	0.93
						28	O	0.63
						29	H	-0.55

References

1. W. S. Hummers and R. E. Offeman, *Journal of the American Chemical Society*, 1958, **80**, 1339-1339.
2. Y. Liu, X. Quan, X. Fan, H. Wang and S. Chen, *Angewandte Chemie International Edition*, 2015, **54**, 6837-6841.
3. W. Kohn and L. J. Sham, *Physical Review*, 1965, **140**, 1133-1138.
4. J. Hafner, *Journal of Computational Chemistry*, 2008, **29**, 2044-2078.
5. G. Kresse and J. Furthmuller, *Physical Review B*, 1996, **54**, 11169-11186.
6. P. E. Blochl, *Physical Review B*, 1994, **50**, 17953-17979.
7. J. P. Perdew, K. Burke and M. Ernzerhof, *Physical Review Letters*, 1997, **78**, 1396-1396.
8. S. Grimme, J. Antony, S. Ehrlich and H. Krieg, *Journal of Chemical Physics*, 2010, **132**, 154104.
9. I. C. Man, H.-Y. Su, F. Calle-Vallejo, H. A. Hansen, J. I. Martinez, N. G. Inoglu, J. Kitchin, T. F. Jaramillo, J. K. Norskov and J. Rossmeisl, *Chemcatchem*, 2011, **3**, 1159-1165.
10. J. K. Norskov, J. Rossmeisl, A. Logadottir, L. Lindqvist, J. R. Kitchin, T. Bligaard and H. Jónsson, *Journal of Physical Chemistry B*, 2004, **108**, 17886-17892.
11. B.-H. Lee, H. Shin, A. S. Rasouli, H. Choubisa, P. Ou, R. Dorakhan, I. Grigioni, G. Lee, E. Shirzadi, R. K. Miao, J. Wicks, S. Park, H. S. Lee, J. Zhang, Y. Chen, Z. Chen, D. Sinton, T. Hyeon, Y.-E. Sung and E. H. Sargent, *Nature Catalysis*, 2023, **6**, 234-243.
12. Q. Zhao, Y. Wang, W.-H. Lai, F. Xiao, Y. Lyu, C. Liao and M. Shao, *Energy & Environmental Science*, 2021, **14**, 5444-5456.
13. K. Jiang, S. Back, A. J. Akey, C. Xia, Y. Hu, W. Liang, D. Schaak, E. Stavitski, J. K. Nørskov, S. Siahrostami and H. Wang, *Nature Communications*, 2019, **10**, 3997.
14. Q. Yang, W. Xu, S. Gong, G. Zheng, Z. Tian, Y. Wen, L. Peng, L. Zhang, Z. Lu and L. Chen, *Nature Communications*, 2020, **11**, 5478.
15. H. Yang, F. Ma, N. Lu, S. Tian, G. Liu, Y. Wang, Z. Wang, D. Wang, K. Tao, H. Zhang and S. Peng, *Nanoscale Horizons*, 2023, **8**, 695-704.
16. C. Ye, Y. Zhou, H. Li and Y. Shen, *Green Chemistry*, 2023, **25**, 3931-3939.
17. H. Shen, N. Qiu, L. Yang, X. Guo, K. Zhang, T. Thomas, S. Du, Q. Zheng, J. P. Attfield, Y. Zhu and M. Yang, *Small*, 2022, **18**, 2200730.
18. C. Liu, H. Li, F. Liu, J. Chen, Z. Yu, Z. Yuan, C. Wang, H. Zheng, G. Henkelman, L. Wei and Y. Chen, *Journal of the American Chemical Society*, 2020, **142**, 21861-21871.